applied optics

Analysis of tunable Faraday rotation angle produced by 1D photonic crystals doped with InSb in the terahertz regime

Tao Zhang,[1,4] Fen-Ying Li,[1] Peng-Xiang Wang,[1] Ming-Yu Mao,[1] Yu Ma,[1] Dan Zhang,[2] and Haifeng Zhang[1,2,3,*]

[1]College of Electronic and Optical Engineering & College of Microelectronics, Nanjing University of Posts and Telecommunications, Nanjing 210023, China
[2]College of Information Science and Technology, Nanjing Forestry University, Nanjing 210037, China
[3]State Key Laboratory of Millimeter Waves of Southeast University, Nanjing 210096, China
[4]e-mail: NjuptZhangTao@163.com
*Corresponding author: hanlor@163.com

Received 28 October 2020; revised 8 January 2021; accepted 18 January 2021; posted 20 January 2021 (Doc. ID 413083); published 10 February 2021

Simple periodic one-dimensional (1D) common photonic crystals (PCs) doped with InSb are proposed to research the Faraday rotation (FR) effect by applying a 4 × 4 transfer matrix method. Analysis indicates that the given 1D PCs can realize a giant FR angle. The influences of the properties of InSb (magnetic induction intensity, temperature, and the length of the InSb layer) and the repeat number of the structure on the FR are investigated due to the tunability of InSb and the features of the structure. Through calculation, it is found that, by adjusting these parameters, we can clearly observe the movement of the extreme values of the FR angle. In addition, the numerical results show that when the magnetic induction intensity and the repeat number of the structure are changed, the FR angle will be significantly altered at the fixed extreme frequency point. Specifically, if the temperature and the thickness of InSb layer are altered, the extreme value of the FR and the frequency point where it happens also will change. We believe these obtained results can provide ideas to design optical isolators and optical switches.

https://doi.org/10.1364/AO.413083

1. INTRODUCTION

The magneto–optical effect (MO) [1–5] is the variety of the optical phenomenon caused between a magnetized substance and light. The magneto–optical effect is a collective concept, which contains the Faraday effect [6–10] and Kerr magneto–optical effect [11–15]. The Faraday effect is a kind of MO rotation effect. The plane of polarization will rotate after a medium magnetized along the optical transmission direction enters plane-polarized light. In 1845, Faraday first observed the MO effect and revealed it for the first time, which showed an interaction between light and a magnetic field. The Faraday effect has an important application in optical isolators [16–18] and optical communications [19–21], and promotes the much deeper research of the physical mechanism of the MO effect and the exploration of new MO materials. MO multilayer film composed of the MO medium and the dielectric periodically arranged has the enhanced characteristics of the Faraday magneto–optical effect, which has aroused widespread interest. In practical applications, the MO crystals [22–26] are widely used to realize the Faraday rotation (FR). In 2020, Kuzmichev *et al.* [27] studied the influence of the position of the plasma nanodisk in the magnetic medium on the Faraday effect, and the experimental results indicated that the magnetic medium inside the nanodisks had the most significant enhancement of the Faraday effect. Moreover, Abdi *et al.* [28] used the 4 × 4 transfer matrix method (TMM) to research the defect mode splitting in proposed one-dimensional (1D) magneto–photonic crystals. It can be found from the simulation results that the defect mode split into two modes for a specific structure cycle number, which provides an application for tunable circular polarization filters. However, for a traditional garnet material series, researchers have developed new materials suitable for the Faraday MO effect. In 2015, Floess *et al.* [29] investigated an ultrathin plasmonic optical rotator made of a EuSe slab and a 1D plasmonic gold grating, and the simulated results showed that the unique dispersion properties of the proposed structure can adjust the wavelengths of the tunable polarization rotation. In 2019, Yasuhara *et al.* [30] studied the Faraday effect in $Tb_2Hf_2O_7$ ceramics and found that the transmittance loss of $Tb_2Hf_2O_7$ is as low as MO material such as terbium gallium

garnet for a great potential application in Faraday equipment in a near-infrared laser.

However, MO materials are widely used in most of the current studies on the FR, and the composition of these mainstream MO materials cannot be separated from the garnet series, which limits the universality of the FR. Research has been done to determine whether or nonmagneto-optical materials can achieve a giant FR. In 2015, Mehdian *et al.* [31] employed a 4×4 TMM to research the MO properties of 1D conjugated photonic crystals (PCs) heterojunctions doping plasma layers, and they found the proposed structure can strongly enhance the FR angle and keep a relatively high transmission, which is beneficial to fabricate tunable filters in the millimeter wave region.

In this paper, a 4×4 TMM is applied to study the FR effect produced by the 1D structure formed between the InSb [32,33] and PCs with high and low refractive indices. InSb is a semiconductor material that aroused widespread interest in scholars because of its excellent tunability in the terahertz (THz) range. The research on the THz field in particular has become a research hotspot in recent years. Due to the tunability of InSb, the influences of the four parameters (temperature T, magnetic induction intensity B, the thickness of the InSb d_p, and the repeat number of the structure period N) on the FR are investigated to realize the enhancement of the FR.

2. SIMULATION MODEL AND CALCULATION METHOD

The transmission of electromagnetic (EM) waves through the proposed 1D PCs doped by InSb is illustrated in Fig. 1. The proposed structure is made up of three dielectrics of A, C, and P. A and C denote two common dielectric layers such as $n_A = 2$ for a high refractive index and $n_C = 1$ for a low refractive index, whose optical thicknesses of layers A and C are expressed as $d_A = \lambda_0/(4n_A)$ and $d_C = \lambda_0/4$, respectively. λ_0 represents the center wavelength selected in this structure and the value of λ_0 is 60 μm. P stands for the semiconductor layer of InSb, and its thickness is $d_p = \lambda_0/(xn_A)$. The corresponding thickness of InSb will change as x takes different values. The proposed 1D PCs doped by InSb are arranged on the order of $(AC)^N$ PA $((CA)^N$, where N signifies the repeat number of the structure period. The structures of 1D PCs are arranged in the z direction. Assuming that the incident EM wave is perpendicular to the surface of the 1D PCs at the surface $Z = Z_0$, the fundamental equation of electromagnetic wave propagation is given by Maxwell equations,

$$\vec{\nabla} \times \vec{E}(\vec{r}, t) = i\omega\mu_0 \vec{H}(\vec{r}, t), \tag{1}$$

$$\vec{\nabla} \times \vec{H}(\vec{r}, t) = -i\omega\varepsilon_0 \hat{\varepsilon} \vec{E}(\vec{r}, t). \tag{2}$$

The dielectric function ε_P of InSb is a nonreciprocal tensor expressed as

$$\boldsymbol{\varepsilon} p = \begin{bmatrix} \varepsilon_1 & i\varepsilon_2 & 0 \\ -i\varepsilon_2 & \varepsilon_1 & 0 \\ 0 & 0 & \varepsilon_3 \end{bmatrix}, \tag{3}$$

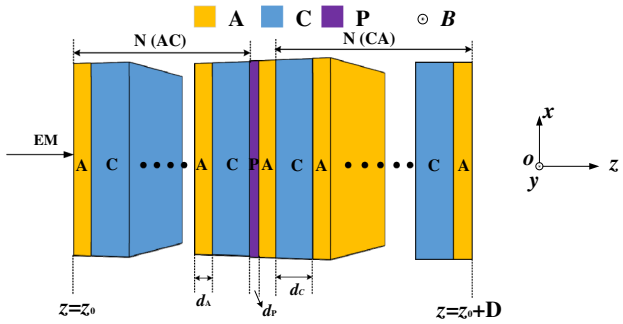

Fig. 1. Schematic illustration of proposed 1D PCs doped with InSb.

$$\varepsilon_1 = \varepsilon_\infty - \varepsilon_\infty \frac{\omega p^2}{\omega(\omega + v_c i)}, \tag{4}$$

$$\varepsilon_2 = -\varepsilon_\infty \frac{\omega p^2 \omega_c}{\omega[(\omega + v_c i)^2 - \omega_c{}^2]}, \tag{5}$$

where $\omega_c = eB/m^*$ expresses the cyclotron frequency. ε_∞ is the high-frequency limit permittivity, and $\varepsilon_\infty = 15.68$. ω is the circular frequency of the incident THz wave. v_c is the collision frequency of carriers, $v_c = e/(\mu 0 m^*) = 0.1\pi$ THz, and ω_P represents the plasma frequency,

$$\omega p = (N_{\mathrm{InSb}} e^2/\varepsilon 0 m^*)^{1/2}, \tag{6}$$

where ε_0 is the free-space permittivity, and N_{InSb} is the intrinsic carrier density. The dielectric property of the InSb greatly depends on the value of N_{InSb}, which is strongly dependent on the temperature T given as

$$N_{\mathrm{InSb}} = 5.76 \times 10^{14} T^{1.5} \exp[-0.26/(2 \times 8.625 \times 10^{-5} \times T)]. \tag{7}$$

The dielectric tensor of the InSb shows the strong dispersion and gyrotropic properties, and it largely depends on the external magnetic field and temperature in the THz range.

When linearly polarized waves propagate parallel to the z axis in the defect layer, right circular polarization (RCP) ε_+ and left circular polarization (LCP) ε_- will appear, whose values can be obtained from the wave equations, $\varepsilon_+ = \varepsilon_1 + \varepsilon_2$ and $\varepsilon_- = \varepsilon_1 - \varepsilon_2$.

The calculation of the FR and transmittance is carried out by adopting the 4×4 TMM, which has been applied and proven to be a valid technique to process the optical properties of magnetic materials. The light field inside each layer is the sum of four normal modes: left and right circularly polarized waves propagating in two directions along the normal of the 1D PCs. After that, a set of 4×4 matrices in response to a layer of the structure is calculated, and the light field value on the boundary of the layer is determined. The amplitudes of the forward and backward propagation modes in the forward and backward directions of the stack are correlated with each other. The entire structure matrix is given by [34]

$$M = [D^{(0)}]^{-1} (S_A S_C)^N S_P S_A (S_C S_A)^N [D^{(0)}], \tag{8}$$

where D and S are the dynamic and block diagonal medium matrices that are given by [34]

$$S=\begin{pmatrix} \cos\beta_+^{(n)} & iN_+^{(n)-1}\sin\beta_+^{(n)} & 0 & 0 \\ iN_+^{(n)}\sin\beta_+^{(n)} & \cos\beta_+^{(n)} & 0 & 0 \\ 0 & 0 & \cos\beta_-^{(n)} & iN_-^{(n)-1}\sin\beta_-^{(n)} \\ 0 & 0 & iN_-^{(n)}\sin\beta_-^{(n)} & \cos\beta_-^{(n)} \end{pmatrix}, \tag{9}$$

$$D=\begin{pmatrix} 1 & 1 & 0 & 0 \\ N_+^{(n)} & -N_+^{(n)} & 0 & 0 \\ 0 & 0 & 1 & 1 \\ 0 & 0 & N_-^{(n)} & -N_-^{(n)} \end{pmatrix}. \tag{10}$$

Here $\beta_j^{(n)}=\frac{\omega}{c}N_j^{(n)}d_n$, $N_j^{(n)}$ $(j=+,-)$, and d_n $(n=\mathrm{A, C, P})$ represents the length and refractive index of right and left circularly polarized wave in n-th layer. It should be known that for dielectric layers $N_+^{(n)}=N_-^{(n)}$, when entire structure matrix $\mathbf{M}$ is known, the transmission can be solved from $t_+=(M_{11})^{-1}$, $t_-=(M_{33})^{-1}$. Then, the total transmission coefficient is $T_1=|t_++t_-|^2/4$. Through the derivation of these expressions, the FR angle is calculated by $\theta_f=\frac{1}{2}\arg(\frac{M_{11}}{M_{33}})$.

3. SIMULATED RESULTS AND DISCUSSION

A. Analysis of FR and Corresponding Transmittance

The diagrams of FR and transmittance in the THz domain for such 1D PCs are given in Fig. 2. Specific parameters are $n_A=2, n_C=1, d_A=\lambda_0/(4n_A), d_C=\lambda_0/4, d_p=\lambda_0/(20n_A)$, $T=175$ K, $B=0.1$ T, and $N=5$, respectively. Figure 2(a) shows that the value of the FR reaches $-21.48°$ with a frequency of 5.69 THz. The relevant transmittance (T_1 appearing at the maximum value of FR) is expressed as $T_1=0.75$ at a frequency of 5.69 THz. This transmission peak is attributed to the defect mode. The mechanism of the Faraday effect can be expounded by the localization of the electric field intensity at such 1D PCs.

To compare the introduction of InSb to enhance the Faraday rotation angle, we introduced a contrast structure that is keeping the original structure unchanged at the time of replacing the InSb material of the P layer with the material of the A layer $((\mathrm{AC})^N\ \mathrm{AA}\ (\mathrm{CA})^N)$ to study the corresponding transmittance and Faraday rotation with the initial conditions $n_A=2$, $n_C=1$, $d_A=\lambda_0/(4n_A)$, $d_C=\lambda_0/4$, $T=175$ K, $B=0.1$ T, and $N=5$, respectively. In Fig. 3, it can be observed that the transmittance reaches 1 at 5 THz, but the Faraday rotation angle is almost 0 in this frequency domain. It reveals that the introduction of InSb can greatly improve the Faraday rotation angle.

B. Effect of Changing Different Parameters on FR

To research the influences of the four parameters (the magnetic induction intensity B, temperature T, the thickness of the InSb d_p, and the repeat number of the structure period N) on the FR and the corresponding transmittance, the relationship between the above parameters on the FR and the corresponding transmittance are illustrated below.

The diagrams of FR and the corresponding transmittance with different B are expressed in Fig. 4 with the specific parameters of $T=175$ K, $d_p=\lambda_0/(20n_A)$, and $N=5$. It is shown

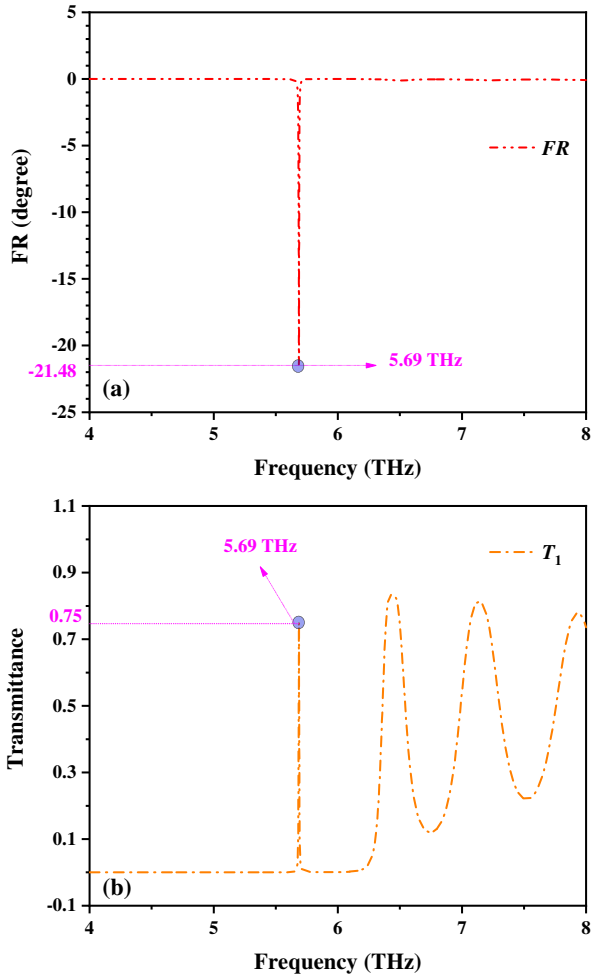

Fig. 2. Diagrams of (a) FR and (b) transmittance in the THz domain for such 1D PCs.

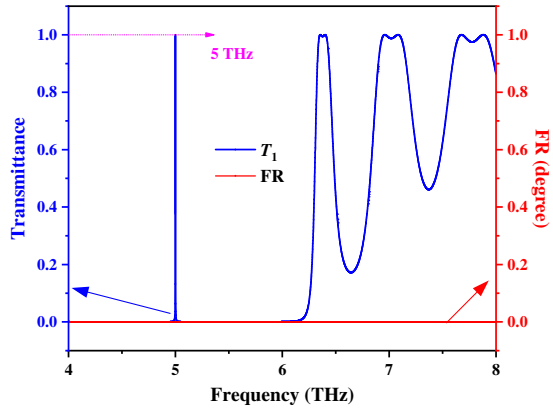

Fig. 3. Diagrams of FR and transmittance in the THz domain for the contrast 1D PCs.

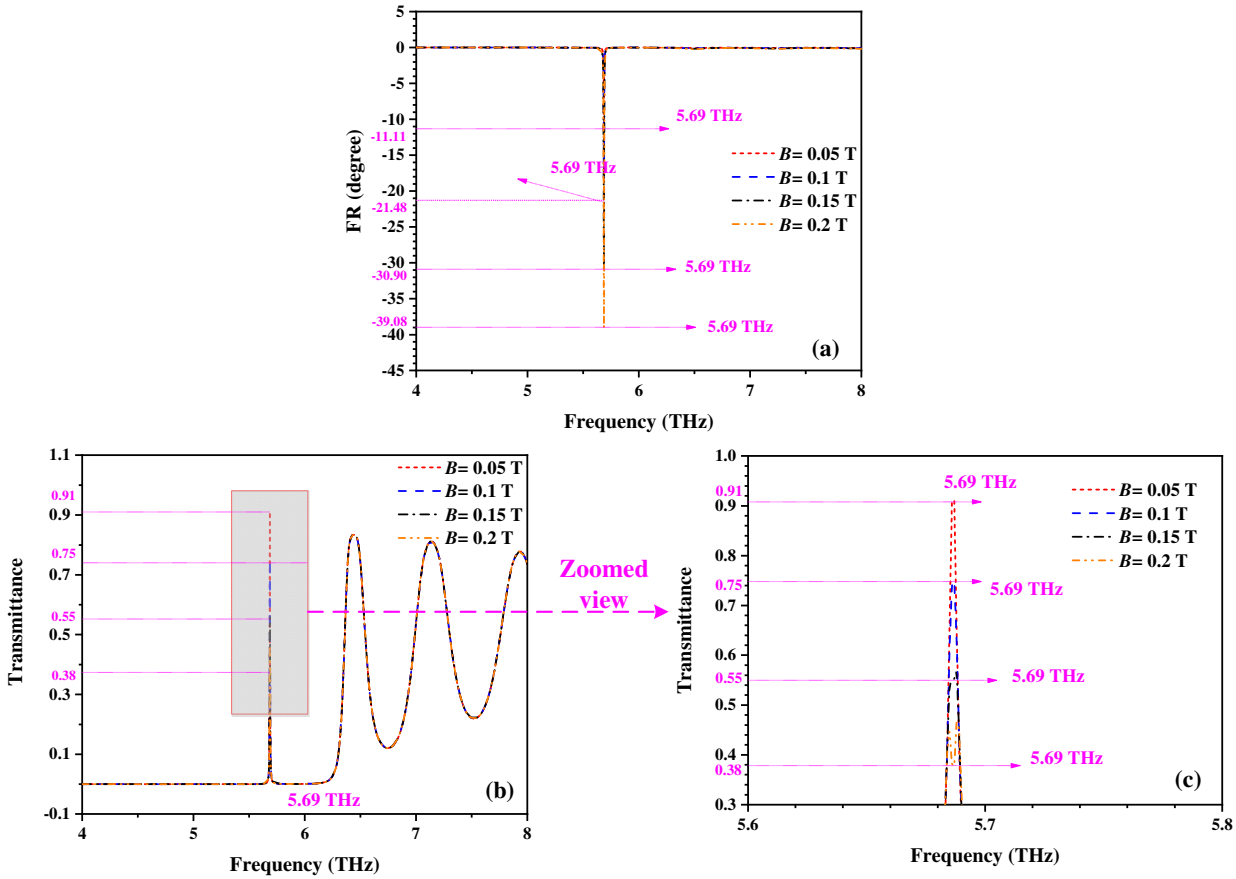

Fig. 4. Diagrams of (a) FR, (b) transmittance, and (c) the partial zoomed view of transmittance in the THz domain with the variety of magnetic induction intensity B for such 1D PCs.

from Fig. 4(a) that the curves of the FR change, evidently emerging at the frequency of 5.69 THz when the magnetic induction intensity B enhances. The greater the magnetic field is, the greater the absolute value of the FR is. Figure 4(a) also shows that when $B = 0.05$ T, $B = 0.1$ T, $B = 0.15$ T, and $B = 0.2$ T, the extreme values of the FR can realize $-11.11°$, $-21.48°$, $-30.90°$, and $-39.08°$, respectively. It shows that for different values of B, the FR is adjustable. Figure 5 shows that if the magnetic field changes from 0.01 to 1.01 T, there is no frequency shift at the extreme value of FR; it only occurs at 5.69 THz. As the magnetic field becomes larger, not only will the value of FR become larger but the bandwidth also will increase. Similarly, it's noted from Figs. 4(b) and 4(c) that when B increases, the curves of corresponding transmittance decline (0.91, 0.75, 0.55, and 0.38) at a frequency of 5.69 THz. It is also observed from Fig. 4(c) that as B increases, the value of the corresponding transmittance not only will drop but also will be divided into two separated peaks as a result of the slight difference of ε_+ and ε_- with the transform of the magnitude of B. In addition, the FR also can be enhanced because of the subtle difference between ε_+ and ε_-.

Figures 6 and 7 are given to explain the above points about the difference between the right and left circularly polarized waves more clearly and intuitively. It can be seen from Fig. 6 that as the magnetic induction intensity B increases, the resonance frequencies for the RCP and LCP waves gradually move to lower

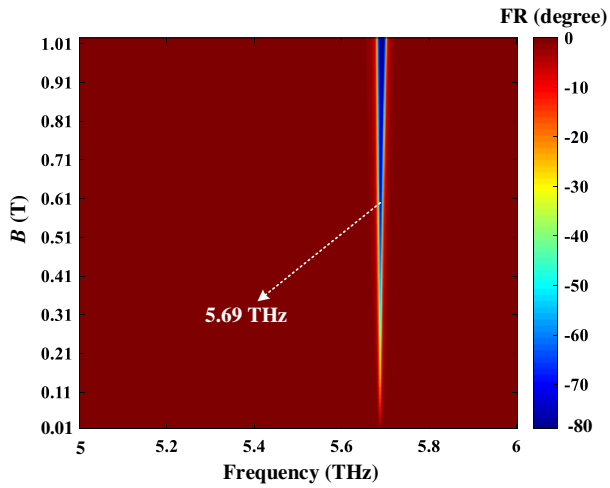

Fig. 5. Diagram of FR for the proposed structure at different B from 0.01 to 1.01 T.

and higher frequencies. The resonance frequency for the LCP wave shifts to 5.684 THz at $B = 0.3$ T, while the resonance frequency for the RCP wave moves to 5.689 THz at $B = 0.3$ T. It's believed that as B continues to increase, the difference between the resonance frequencies for RCP and LCP waves will become larger. Figure 7 also shows that the phase angle reaches 0.20°

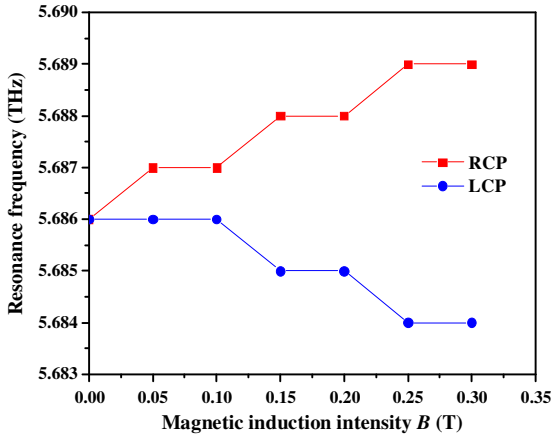

Fig. 6. Transformation of resonance frequencies for RCP and LCP waves with the variety of magnetic induction intensity B.

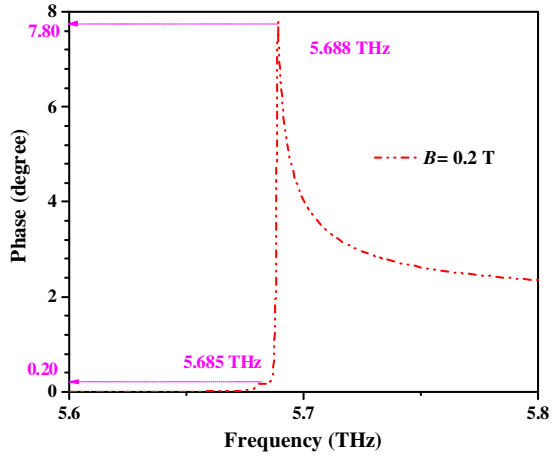

Fig. 7. Diagram of the phase of transmittance with $B = 0.2$ T.

at 5.685 THz and 7.80° at 5.688 THz with $B = 0.2$ T. The phase difference between the two frequency points is 7.60°, which can be negligible (since the change of B has little effect on the phase, and Fig. 7 only shows the case of $B = 0.2$ T). The negligible phase difference provides an explanation for the small peak difference of the twin peaks.

To investigate the effects of temperature T on the FR, the diagrams of the FR and the corresponding transmittance in the THz domain with different temperatures are plotted in Fig. 8. The other parameters are $B = 0.1$ T, $d_p = \lambda_0/(20n_A)$, and $N = 5$, respectively. It can be observed from Fig. 8(a) that the curves of the FR move to the higher frequencies when the temperature rises. If $T = 165$ K, $T = 175$ K, $T = 185$ K, and $T = 195$ K, the extreme values of the FR can reach −12.05°, −21.48°, −36.73°, and −52.39° at frequencies of 5.68 THz, 5.69 THz, 5.70 THz, and 5.73 THz, respectively, which means that temperature can affect the FR. Figure 9 shows that the FR curve extends to the higher frequencies. The color of the

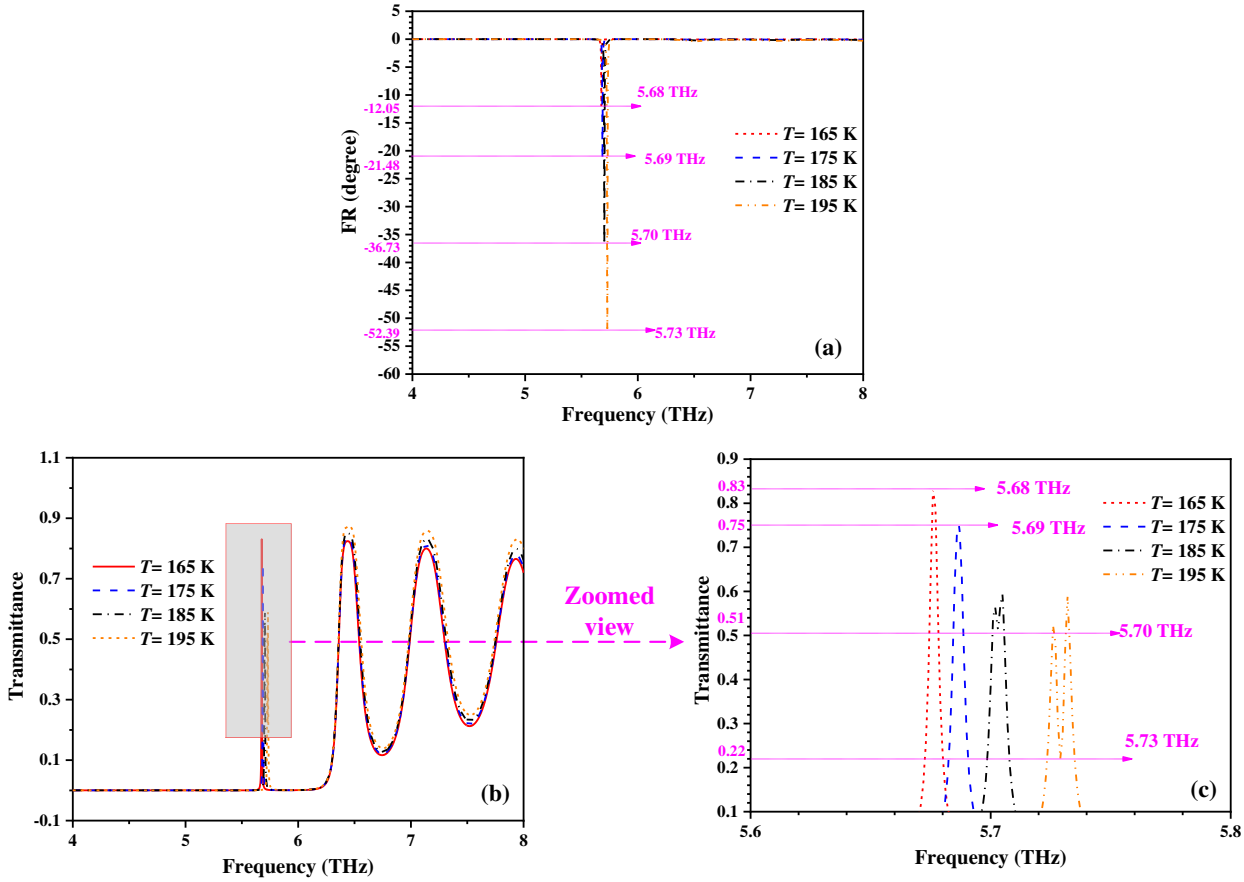

Fig. 8. Diagrams of (a) FR, (b) transmittance, and (c) partial zoomed view of transmittance in the THz domain with a variety of temperatures for such 1D PCs.

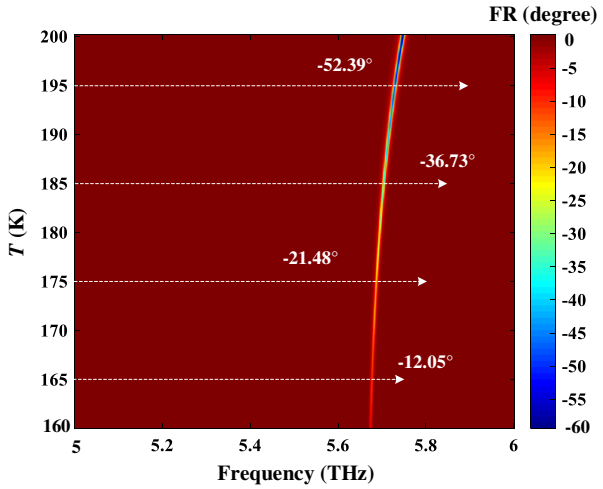

Fig. 9. Diagrams of FR for the proposed structure at different T from 160 to 200 K.

value of the FR becomes darker, indicating the higher value of the FR, which is consistent with the results of the analysis. The diagrams of transmittance and its partial zoomed view are offered in Fig. 8(c). It can be seen from Fig. 8(c) that when the temperature rises, the corresponding transmittance decreases. When $T = 165$ K, $T = 175$ K, $T = 185$ K, and $T = 195$ K, the corresponding transmittance can achieve 0.83, 0.75, 0.51, and 0.22 which appear at 5.68 THz, 5.69 THz, 5.70 THz, and 5.73 THz, respectively. It is obvious from Eqs. (6) and (7) that changing the temperature will affect the plasma frequency ω_p. Then, the alteration of the refractive index of InSb also affects the optical length of the defect mode and the different resonance frequencies are shown in Fig. 8. In addition, when the temperature enhances, two separated peaks are obtained, as shown in in Fig. 8(c), due to the slight difference between the RCP ε_+ and the LCP ε_- resulting from the transform of the temperature.

Similar to the influences on the FR with different temperatures, the simulation results show that the variety of the thickness of InSb d_p also has an effect on the FR, which can be noted from Fig. 10 with specific parameters $T = 175$ K, $B = 0.1$ T, and $N = 5$. As shown in Fig. 10(a), the absolute value of the FR decreases when d_p falls. It can be seen from the graph in Fig. 10(a) that when $d_p = \lambda_0/(18n_A)$, $d_p = \lambda_0/(20n_A)$, $d_p = \lambda_0/(22n_A)$, and $d_p = \lambda_0/(24n_A)$, the FR is found at 5.63 THz, 5.69 THz, 5.74 THz, and 5.78 THz, whose extreme values are $-26.88°$, $-21.48°$, $-17.88°$, and $-14.35°$, respectively. This proves that the thickness of InSb d_p has a significant impact on the value of the FR. Similar to the effect of temperature, the change of the thickness of the defect mode will also cause a shift of the FR extreme frequency point. In other words, when x becomes larger, d_p becomes smaller, the absolute value of FR becomes smaller, and the frequency point at the extreme value moves to a higher frequency, as shown in Fig. 11. As displaced in Fig. 10(b), the corresponding transmittance becomes larger as d_p drops with detailed trends: If $d_p = \lambda_0/(18n_A)$, $d_p = \lambda_0/(20n_A)$, $d_p = \lambda_0/(22n_A)$, and $d_p = \lambda_0/(24n_A)$, the corresponding transmittance is 0.65, 0.75, 0.83, and 0.88, which is located at 5.63 THz, 5.69 THz, 5.74 THz, and 5.78 THz, respectively. Such a phenomenon can

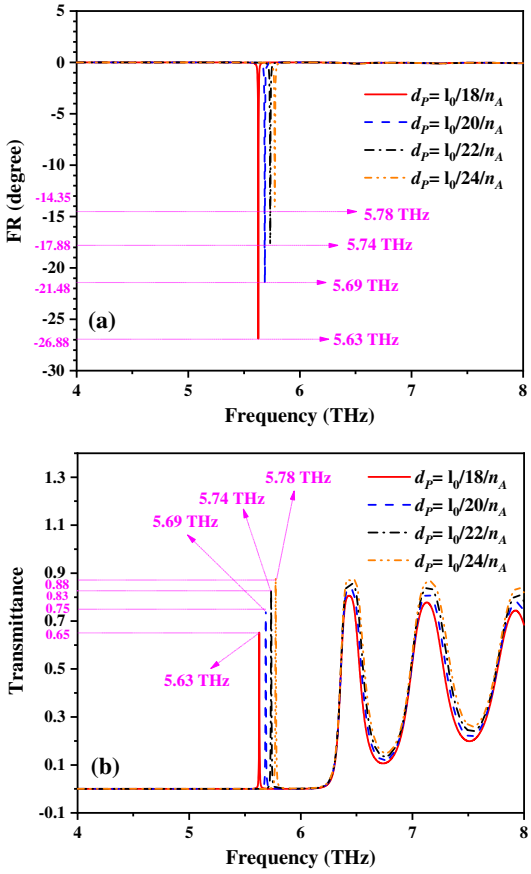

Fig. 10. Diagrams of (a) FR and (b) transmittance in the THz domain with the variety of the thickness of InSb d_p for such 1D PCs.

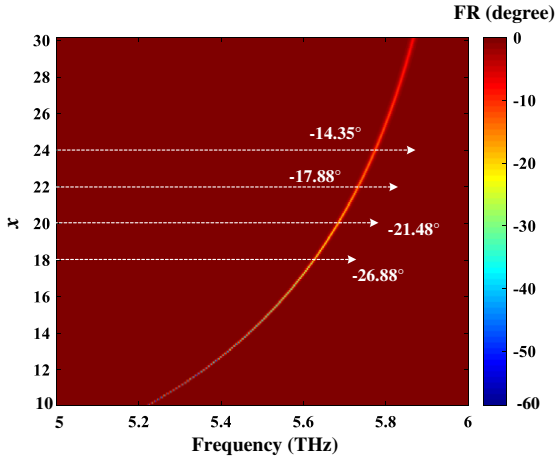

Fig. 11. Diagrams of Faraday rotation for the proposed structure at different x from 10 to 30.

be explained by the following principle: When the InSb layer that causes the FR effect becomes thicker, the electromagnetic wave passing through the proposed 1D PCs will cause enhancement of the FR. Consequently, the corresponding transmittance will decrease as the thickness of the defect layer increases.

The FR and the corresponding transmittance with the variety of the repeat number of N are plotted in Fig. 12 with specific parameters: $T = 175$ K, $B = 0.1$ T, and $d_p = \lambda_0/(20n_A)$. As

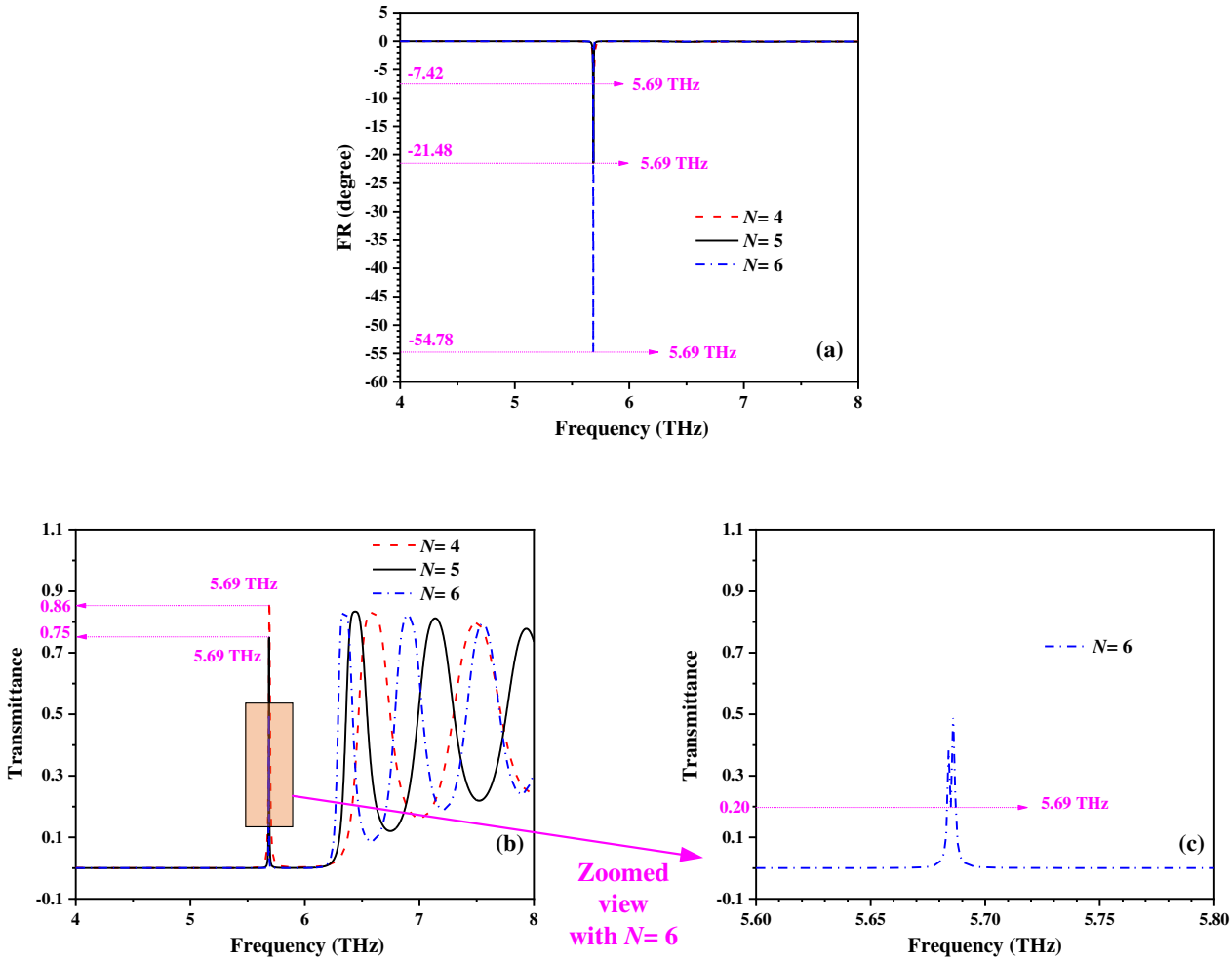

Fig. 12. Diagrams of (a) FR and (b)–(c) transmittance in the THz domain with a variety of the repeat number of N for such 1D PCs.

depicted in Fig. 12, when N increases, the frequency points of curves for the FR and the corresponding transmittance do not move, and the value of the FR rises, but the corresponding transmittance declines. It can be noted from Fig. 12(a) that if $N = 4$, 5, and 6, the extreme values of FR can reach $-7.42°$, $-21.48°$, and $-54.78°$ at the frequency of 5.69 THz, respectively. It reveals that the repeat number N makes a marked enhancement to the FR. This unique characteristic is due to the light localization, and the multiple interference of light is in the mode layer. From Fig. 12(b), it can also be seen that when $N = 4$, 5, and 6, the corresponding transmittance achieves 0.86, 0.75, and 0.20 at the frequency of 5.69 THz, respectively. This means an increase in N will decrease the value of transmittance [the zoomed view can be seen in Fig. 12(c)].

4. CONCLUSION

In short, 1D PCs doped with InSb are constructed to produce a giant FR by using a 4×4 TMM. Analysis indicates that the proposed 1D PCs can realize a tunable FR according to the properties of InSb in the THz regime. Those parameters (magnetic induction intensity B, temperature T, the thickness of InSb d_p, and the repeat number of N) have an obvious impact on the FR. Through numerical calculation, it is found that by adjusting temperature T and the thickness of InSb d_p, the extreme value of FR will be altered, along with the frequency point where the extreme value of the FR occurs changes. It is worth mentioning that when the value of T or d_p becomes larger, its extreme value also becomes larger, but the frequency point at the extreme value moves to the lower frequencies for d_p and to the higher frequencies for T. Moreover, FR changes significantly at the fixed extreme frequency point for changing B and N. We believe the proposed 1D PCs can be used to design optical isolators and optical switches.

Funding. Open Research Program in China's State Key Laboratory of Millimeter Waves (K201927).

Disclosures. The authors declare no conflicts of interest.

REFERENCES

1. Y. L. Li, T. F. Li, Q. Y. Wen, and F. Fan, "Terahertz magneto-optical effect of wafer-scale La: yttrium iron garnet single-crystal film with low loss and high permittivity," Opt. Express **28**, 21062–21071 (2020).

2. B. Laure, G. Emilie, R. Francois, N. Soehie, and J. Damien, "Longitudinal magneto-optical effect enhancement with high transmission through a 1D all-dielectric resonant guided mode grating," Opt. Express **28**, 8436–8444 (2020).
3. K. Habanjar, M. Almoussawi, A. M. Abdallah, and R. Awad, "Magneto-optical effect of (Sm, Co) co-doping in ZnO semiconductor," Physica B **598**, 412444 (2020).
4. H. Liu, H. Y. Lin, J. J. Ruan, D. Sun, and L. M. Song, "A special intracavity power-modulator using the TGG magneto-optical effect," Optik **212**, 164739 (2020).
5. W. X. Feng, J. P. Hanke, X. D. Zhou, G. Y. Guo, B. Stefan, M. Yuriy, and Y. G. Yao, "Topological magneto-optical effects and their quantization in noncoplanar antiferromagnets," Nat. Commun. **11**, 118 (2020).
6. G. Y. Bai, L. J. Dong, S. Feng, and Z. F. Feng, "Faraday effects in one-dimensional magneto-optical photonic crystal," Opt. Mater. **35**, 252–256 (2012).
7. S. Y. Yin, J. Lousteau, M. Olivero, M. Merlo, N. Boetti, S. Abrate, Q. L. Chen, Q. P. Chen, and D. Milanese, "Analysis of Faraday effect in multimode tellurite glass optical fiber for magneto-optical sensing and monitoring applications," Appl. Opt. **51**, 4542–4546 (2012).
8. V. Morozhenko, V. Maslov, and N. Kachur, "Manifestation of the Faraday effect in non-polarized light under optical resonance conditions," Opt. Commun. **426**, 423–426 (2018).
9. I. Snetkov, A. Yakovlev, D. Permin, and S. S. Balabanov, "Magneto-optical Faraday effect in dysprosium oxide (Dy_2O_3) based ceramics obtained by vacuum sintering," Opt. Lett. **43**, 4041–4044 (2018).
10. I. V. Bychkov, D. A. Kuzmin, V. A. Tolkachev, and P. S. Plaksin, "Plasmon mediated inverse Faraday effect in a graphene–dielectric–metal structure," Opt. Lett. **43**, 26–29 (2018).
11. M. Amanollahi and M. Zamani, "Performance of transverse magneto-optical Kerr effect in double-positive, double-negative and single-negative bi-gyrotropic metamaterials," J. Magn. Magn. Mater. **502**, 166451 (2020).
12. R. François, V. Bobin, G. Emilie, N. Soehie, J. Yves, and J. Damien, "Enhancement of both Faraday and Kerr effects with an all-dielectric grating based on a magneto-optical nanocomposite material," ACS Omega **5**, 2886–2892 (2020).
13. E. Moncada-Villa and J. R. Mejía-Salazar, "High-refractive-index materials for giant enhancement of the transverse magneto-optical Kerr effect," Sensors **20**, 952 (2020).
14. M. Amanollahi, E. Moncada-Villa, and M. Zamani, "Bi-gyrotropic impact upon high-performance transverse magneto-optical Kerr effect in a superlens," J. Magn. Magn. Mater. **484**, 234–237 (2019).
15. O. V. Borovkova, F. Spitzer, V. I. Belotelov, L. A. Akimov, A. N. Poddubny, G. Karczewski, M. Wiater, T. Wojtowicz, A. K. Zvezdin, D. R. Yakovlev, and M. Bayer, "Transverse magneto-optical Kerr effect at narrow optical resonances," Nanophotonics **8**, 287–296 (2019).
16. E. Genin, M. Mantovani, G. Pillant, C. D. Rossi, L. Pinard, C. Michel, M. Gosselin, and J. Casanueva, "Vacuum-compatible low-loss Faraday isolator for efficient squeezed-light injection in laser-interferometer-based gravitational-wave detectors," Appl. Opt. **57**, 9705–9713 (2018).
17. H. Kato, T. Matsushita, A. Takayama, and M. Egawa, "Properties of one-dimensional magnetophotonic crystals for use in optical isolator devices," IEEE Trans. Magn. **38**, 3246–3248 (2002).
18. S. Sakaguchi and N. Sugimoto, "Multilayer films composed of periodic magneto-optical and dielectric layers for use as Faraday rotators," Opt. Commun. **162**, 64–70 (1999).
19. M. A. Kabir, K. Ahmed, M. M. Hassan, and M. M. Hossain, "Design a photonic crystal fiber of guiding terahertz orbital angular momentum beams in optical communication," Opt. Commun. **475**, 126192 (2020).
20. W. Yang and Y. S. Lin, "Tunable metamaterial filter for optical communication in the terahertz frequency range," Opt. Express **28**, 17620–17629 (2020).
21. I. Amiri, A. N. Z. Rashed, H. M. A. Kader, A. Al-Awamry, I. A. A. El-Aziz, P. Yupapin, and G. Palai, "Optical communication transmission systems improvement based on chromatic and polarization mode dispersion compensation simulation management," Optik **207**, 163853 (2020).
22. D. X. Dong, Y. W. Liu, Y. Fei, and Y. Q. Fan, "Enhancing the Faraday rotation in the monolayer phosphorus base of magneto-photonic crystals," Opt. Mater. **102**, 109809 (2020).
23. D. Nassim, M. Bouras, and A. Kahlouche, "Magneto-photonic crystal micro-cavities in one dimensional photonic crystals fabricated by sol gel process," J. Nanoelectron. Optoelectron. **14**, 1189–1193 (2019).
24. B. S. Darki and A. Z. Nezhad, "Magneto-optical properties of asymmetric one-dimensional magneto-photonic crystals," J. Opt. **21**, 015101 (2018).
25. T. Jalali and M. Hessamodini, "The effect of 1D magneto-photonic crystal defect mode on Faraday rotation," Optik **126**, 3954–3958 (2015).
26. S. Hamidi, M. M. Tehranchi, and M. Shasti, "Engineered one-dimensional magneto-photonic crystals for wavelength division multiplexing systems," J. Phys. D **44**, 205107 (2011).
27. A. N. Kuzmichev, D. Sylgacheva, M. A. Kozhaev, and D. Krichevsky, "Influence of the plasmonic nanodisk positions inside a magnetic medium on the Faraday effect enhancement," Phys. Status Solidi (RRL) **14**, 1900682 (2020).
28. R. Abdi and A. Namdar, "Circular polarization bandpass filters based on one-dimensional magnetophotonic crystals," J. Mod. Opt. **60**, 1619–1626 (2013).
29. D. Floess, J. Y. Chin, A. Kawatani, and D. Dregely, "Tunable and switchable polarization rotation with non-reciprocal plasmonic thin films at designated wavelengths," Light Sci. Appl. **4**, e284 (2015).
30. R. Yasuhara and A. Ikesue, "Magneto-optic pyrochlore ceramics of Tb2Hf 2O7 for Faraday rotator," Opt. Express **27**, 7485–7490 (2019).
31. H. Mehdian, Z. Mohammadzahery, and A. Hasanbeigi, "Magneto-optical properties of one-dimensional conjugated photonic crystal heterojunctions containing plasma layers," Appl. Opt. **54**, 7949–7956 (2015).
32. S. Chen, F. Fan, X. H. Wang, and P. F. Wu, "Terahertz isolator based on nonreciprocal magneto-metasurface," Opt. Express **23**, 1015–1024 (2015).
33. X. Y. Dai, Y. J. Xiang, S. C. Wen, and H. Y. He, "Thermally tunable and omnidirectional terahertz photonic bandgap in the one-dimensional photonic crystals containing semiconductor InSb," J. Appl. Phys. **109**, 053104 (2011).
34. H. Mehdian, Z. Mohammadzahery, and A. Hasanbeigi, "Tunable Faraday effect in one-dimensional photonic crystals doped by plasma," Optik **127**, 3895–3898 (2016).